

An Automatic and Forward Method to Establish 3-D Parametric Scattering Center Models of Complex Targets for Target Recognition

Jin Liu[✉], Siyuan He, Member, IEEE, Lei Zhang[✉], Yunhua Zhang,
Guoqiang Zhu, Member, IEEE, Hongcheng Yin, and Hua Yan

Abstract—In this article, an automatic and forward method is realized to establish attributed scattering center models directly from the computer-aided design (CAD) model of the complex target. The main steps include the preprocessing of the CAD model, the separation of scattering sources, the selection of strong scattering sources, and the automatic determination of model parameters. With the proposed method, the scattering sources, scattering mechanisms, and model parameters of the scattering centers can be identified and derived, such that the complicated manual intervention is completely avoided. Moreover, the method establishes the distributed scattering center models formed by curved surfaces with large curvature radii. Therefore, the formation mechanism of the distributed scattering center is extended from typical scattering structures to a general case. Thus, the model of the attributed scattering center is extended and can be applied to describe the scattering from the real structures of the complex target. The geometric shape of the scattering source is distinguished based on the principal curvature radii, which are calculated by differential geometry theory. Thus, the frequency dependence parameter is obtained according to its corresponding relationship with the geometric shape. In addition, based on the automatic method, a technology is studied to diagnose and correct the scattering center models of a target whose CAD model is unknown or partially known. Finally, parametric models of several targets in the Moving and Stationary Target Acquisition Recognition (MSTAR) program are established, and then compared with the measured data. The results validate the effectiveness of the proposed method.

Index Terms—Automatic modeling, automatic target recognition (ATR), ray tracing, scattering center, scattering mechanism.

I. INTRODUCTION

IN RECENT years, the model-based automatic target recognition (ATR) of synthetic aperture radar (SAR) images [1]–[7] has attracted great attention due to its reduced storage requirement and flexible extended operation conditions. The Moving and Stationary Target Acquisition and Recognition (MSTAR) [1], [2] system is a typical representative of the latest model-based ATR methods, which recognize

Manuscript received October 22, 2019; revised December 28, 2019; accepted April 2, 2020. Date of publication May 12, 2020; date of current version November 24, 2020. This work was supported by the National Natural Science Foundation of China under Grant 61571333 and Grant 61301061. (*Corresponding author: Siyuan He*)

Jin Liu, Siyuan He, Lei Zhang, Yunhua Zhang, and Guoqiang Zhu are with the School of Electronic Information, Wuhan University, Wuhan 430072, China (e-mail: starty@whu.edu.cn; siyuanhe@whu.edu.cn).

Hongcheng Yin and Hua Yan are with the National Electromagnetic Scattering Laboratory, Beijing 100854, China.

Color versions of one or more of the figures in this article are available online at <https://ieeexplore.ieee.org>.

Digital Object Identifier 10.1109/TGRS.2020.2989856

targets by matching the features extracted from measurement with those predicted from target feature database. Therefore, the construction of the target feature database is the key stage in the model-based SAR ATR system. In high frequency, the scattering of an electrically large target can be well approximated as a sum of response from individual scattering centers [23]. The scattering center model enables a concise description of radar targets and reflects the electromagnetic scattering characteristics of the targets, indicating that it can form the target feature database well. Therefore, how to establish the scattering center model of the target will directly affect the efficiency of ATR.

Numerous researches on the scattering center model have been studied. Potter and Moses [8] first proposed an attributed scattering center model, which can reflect the dependence of the backscattered field on frequency and azimuth. Subsequently, considering the dependence of the scattering field on azimuth more fully, Gerry *et al.* [9] improved the attributed scattering center model. Thus, the model parameters have clear physical interpretations and can well describe target shape, pose, and position. From then on, various methods for establishing the attributed scattering center model have been proposed. In fact, the attributed scattering center extraction is equivalent to the model parameter estimation from radar measurements. Koets and Moses [10], [11] studied a method for extracting the attributed scattering center directly from SAR images, and estimating the physically relevant parameters locally from data in the high energy region of the SAR image. Akyildiz and Moses [12] estimated the model parameters of attributed scattering centers from an SAR image. By model fitting only on regions of the image, the computational complexity was reduced significantly. Liu *et al.* [13] proposed a new algorithm to extract the attribute scattering centers and estimate their model parameters from a measured SAR image based on the sparse representation with dictionary refinement. The parametric scattering center model represented by the attributed scattering center model has wide application prospects in the model-based ATR [14], [25]–[29]. Chiang and Moses [14] studied a method for classification performance estimation for SAR ATR based on the attributed scattering center model.

The studies mentioned above established the scattering center model by inverse methods, in other words, position, intensity, and frequency feature of the scattering center are extracted from the measured or simulated data (e.g., SAR

image) by inverse optimization [5], [9]–[17]. Therefore, it is difficult for the scattering center model to provide a physically relevant description, as well as a corresponding relationship with the actual structures of the target. More importantly, the inversion process consumes much computational time and storage. He *et al.* [24] first proposed a forward approach to establish parametric scattering center models for radar target. The scattering center models can be obtained directly from a computer-aided design (CAD) model of the target through the theoretical analysis of electromagnetic scattering mechanism, which is an analytic approach. And the scattering center models obtained by this approach have clear correspondence with the local structures of the target. Therefore, this approach provided an effective and concise database for model-based ATR, and attracted wide research attention since proposed.

However, the modeling objects in [24] are targets with relatively simple geometric models. Besides, it requires extensive professional manual intervention in obtaining the scattering source, the type of scattering center, and the model parameters. For example, the method in [24] can only establish the distributed scattering center model formed by typical structures (e.g., cylinder and dihedral). Moreover, it requires professionals to identify a distributed scattering center and calculate its length parameter with the CAD model at each modeling attitude. In order to determine the frequency dependence parameter, the scattering mechanism of the scattering source is also distinguished by professionals according to the target's CAD model. But obviously it is very difficult to manually distinguish the scattering mechanism of the complex target at different attitudes. Besides, a large number of scattering center models for complex targets also need to be established in the process of target recognition. Therefore, the previous method will not meet the modeling object and efficiency, and it is urgent to improve the forward approach and turn it into a method that is automatically executed by a computer.

This article realizes an automatic and forward method to establish scattering center models for the complex target. Meanwhile, a set of automatic approaches is developed to determine the frequency dependence parameter and the more general length parameter of the scattering center. The frequency dependence parameters are automatically obtained by distinguishing the surface shape of the scattering structure. More importantly, this article extends the scattering mechanism of distributed scattering centers from typical scattering structures and specular reflection mechanism to a more general scattering case. With the given parameters of radar attitude, two endpoints are selected from the equivalent reflection points of all contributive rays, which are determined based on the optical path difference equivalence principle [24]. Then, the length parameter is obtained by calculating their distance. Based on the method mentioned above, the code, which is called the Forward Modeling of Parametric Scattering Center Model module (FMPM), is consequently developed.

In addition, a technology is studied to diagnose and correct scattering center models of a target whose CAD model is unknown or partially known in this article. Up until now, very few studies on establishing the scattering center models of the unknown target have been reported. There are two

main reasons: one is that the radar is difficult to provide sufficient and available measurement data of the unknown target. Another is that the traditional inversion modeling method has insufficient ability to establish the correspondence between the scattering center and the target structure. However, due to the advantages of high modeling efficiency and clear correspondence between the scattering center and the scattering structure, the automatic and forward method has the potential to diagnose and correct scattering center models of a target whose CAD model is unknown or partially known. An experiment of the T72 is given to illustrate the validity of the technology. Because the real CAD model of T72 is difficult to obtain, the scattering center models established from an assumed model need to be corrected according to the measurement data through modifying structures of the CAD model, thus improving the accuracy of the scattering center models.

Finally, the parametric scattering center models of several targets in the MSTAR data set are established by the FMPM. The reconstructed characteristics of the scattering center models are compared with the measured data provided by the MSTAR data set, and the results verify the effectiveness of this method. Accordingly, the scattering center models can provide a database for feature matching of the SAR ATR system. Ding and Wen [25], [26] used the features reconstructed from these scattering center models to match those extracted from the measurements to distinguish targets, finally accomplished model-based target recognition. Yang *et al.* [27]–[29] used the three-dimensional (3-D) scattering center models to estimate absolute attitude by combining the parametric motion model.

The main contributions of this article are summarized as follows.

- 1) An automatic and forward method is realized to establish the parametric scattering center model of complex targets. In addition, the modeling code, which is called the FMPM, is also developed. Only the CAD model of the complex target needs to be input, the scattering centers can be output, as well as their physically relevant parameters.
- 2) A set of automatic approaches is developed to determine the more general length parameter and the frequency dependence parameter of the scattering center. The scattering mechanism of the distributed scattering center is expanded from typical scattering structures and specular reflection mechanism to a more general case, thus establishing the distributed scattering center models formed by curved surfaces with large curvature radii. The frequency dependence parameter is determined by the principal curvature radii of the component surface, which are calculated with differential geometry theory, thus avoiding the complicated artificially prejudgment of the scattering mechanism.
- 3) A technology is studied to diagnose and correct scattering center models of the targets whose CAD models are unknown or partially known. Since the modeling method in this article is automatic and rapid, and the correspondence between the scattering center and the scattering structure is much clearer, it can be applied to improve the accuracy of the scattering center models

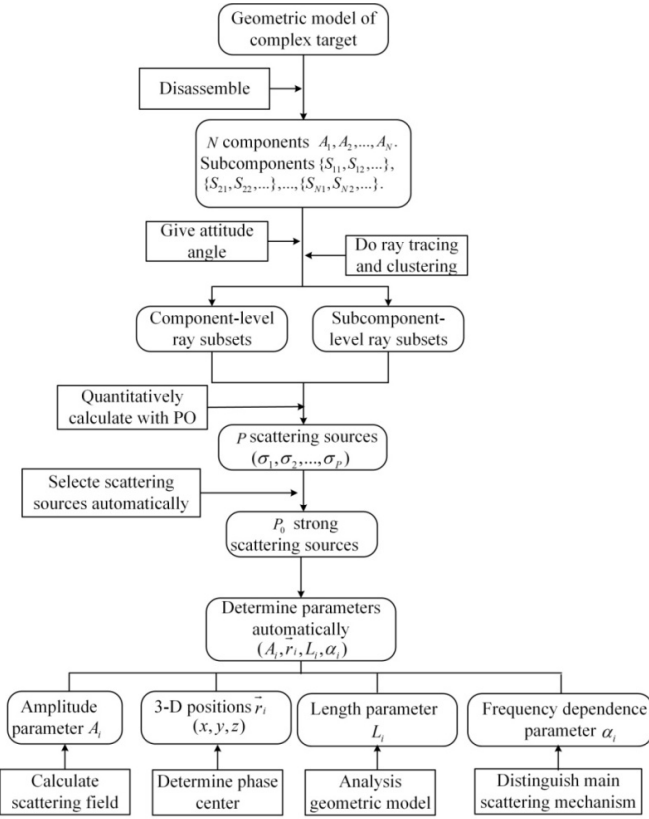


Fig. 1. Flowchart of establishing parametric scattering center model for a complex target.

by modifying the geometric structure and configuration of an assumed CAD model according to measured or simulated data. It can be expected that this technology will play an important role in target recognition.

The remainder of this article is organized as follows. Section II introduces the automatic method to establish the parametric scattering center model for a complex target. The main steps include the preprocessing of the CAD model, the separation of scattering sources, the selection of strong scattering sources, and the automatic determination of model parameters. And the determinations of the more general length parameter and the frequency dependence parameter are the focus of this article. In Section III, a technology is presented to diagnose and correct scattering center models of the unknown targets. In Section IV, the parametric scattering center models of several targets are established by the automatic method. The reconstructed characteristics are consequently compared with the reference data provided by MSTAR or other reliable database, and the results of this method are verified. Then, an experiment on T72 is conducted to illustrate the validity of the correction technology. Finally, in Section V, the conclusion is drawn with some further discussions.

II. METHOD OF ESTABLISHING SCATTERING CENTER MODEL

This article realizes an automatic and forward method to obtain the parametric scattering center model for the complex target. The flowchart of our method is shown in Fig. 1.

The detailed procedure is as follows. The first step is the preprocessing of the CAD model. The CAD model is meshed with small triangular facets. Then component decomposition is done for the target surface, and numbered components and subcomponents are obtained. Each component usually contains several subcomponents. After completion of preprocessing, the entire parametric modeling process will be automatically performed at entire attitudes. The second step is the separation of scattering sources. Based on the ray tracing and clustering with physical optics (PO) technology, several single-reflected ray subsets and multiple-reflected ray subsets are clustered from the total scattering field of the target. Here, the ray subsets are the physical form of candidate scattering sources. The third step is the selection of the scattering sources. The candidate scattering sources are sorted according to their scattering contributions, and the strong scattering sources are selected. The fourth step is the determination of physically relevant parameters. This article extends the scattering mechanisms of distributed scattering centers from typical scattering structures and specular reflection mechanism to a more general scattering case, and can establish the distributed scattering center models formed by curved surfaces with large curvature radii. With the given parameters of radar attitude (e.g., azimuth direction), two equivalent reflection endpoints of all contributive rays are selected, thus obtaining the length parameter by calculating their distance. The frequency dependence parameter is closely related to the geometric structure of the scattering source. In this article, the principal curvature radii are calculated by differential geometry theory to determine the geometric shape of the surface, and then the corresponding frequency dependence parameters are obtained. The amplitude parameter has been calculated by ray tracing with PO. In addition, the 3-D positions represent the phase center of the scattering center, which can be determined based on the optical path difference principle.

A. Method of Obtaining Scattering Center

To directly separate scattering sources from the CAD model of the complex target and establish a foundation for parameter determination, an important preprocessing step is disassembling the CAD model. The target is modeled with small triangular facets. To make electromagnetic calculation quickly and effectively, the reasonable model simplification is necessary. Then, the component decomposition is done referring to the variation of target surface normal and electrically large size, and the decomposed components are marked as A_1, A_2, \dots, A_N . Thus, all facets can be clustered according to their affiliated components. In addition, to identify the dominant scattering region of the components, each component $A_i, i = 1, 2, \dots, N$ is decomposed into a group of subcomponents and marked as S_{i1}, S_{i2}, \dots . Therefore, each facet contains information about the marks of their affiliated components and subcomponents, as well as other geometric information. Fig. 2 shows the sketches of the decomposed components and decomposed subcomponents of the Sandia Laboratories implementation of cylinders (SLICY).

The second step is the separation of scattering sources. After model preprocessing, the scattering sources are separated and

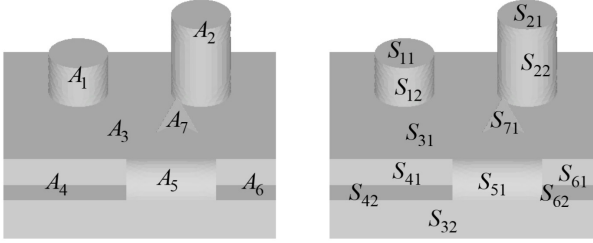


Fig. 2. (Left) Sketches of component. (Right) Subcomponent of SLICY.

quantitatively characterized by the ray tracing and clustering with the PO technique. The incident plane waves are represented with a set of space rays, which is marked as T . Then, the paths of all rays in T are recorded with the marks of the components and subcomponents. Therefore, the rays can be clustered as ray subsets at the component level and subcomponent level according to the paths. The component-level ray subset is marked as U_i , and the subcomponent-level ray set in U_i is marked as V_{ij} . Here, $T \sim \sum_{i=1}^P U_i$ and $U_i \sim \sum_{j=1}^M V_{ij}$, where P is the number of the component-level ray sets, and M is the number of the subcomponent-level ray sets in U_i . The component-level ray subsets are the physical forms of the scattering centers [24]. Meanwhile, the scattering field of each ray subset is calculated by the PO method.

The third step is the selection of the scattering sources. After separating and quantitatively characterizing the P candidate scattering sources, in order to simplify the scattering center model of the complex target, it is necessary to discard the scattering sources with weaker scattering fields and retain the scattering sources with stronger scattering fields. The selection process is as follows. First, the total field of the target is calculated as a reference value. Then, the P candidates are sorted according to the descending order of the scattering fields, and the stronger scattering sources which are at the top of the sorted queue are preselected. The sum of the scattering fields of these scattering sources is compared with the reference value. If the relative error satisfies the precision requirement of modeling, these stronger scattering sources are considered to describe the electromagnetic backscattering of the target successfully. Otherwise, a new scattering source must be added from the remaining candidates until the relative error is satisfied. Generally, the higher the precision is, the more the weaker scattering sources need to be included. Finally, P_0 scattering centers are obtained. Note that the scattering centers are separated and selected automatically by the FMPM. Simultaneously, the dominant subcomponent that contributes the most to the component is identified according to its scattering contribution. The dominant subcomponent will help to the scattering mechanism analysis and parameter determination.

Compared with the reverse extraction methods, the scattering centers are obtained completely from the CAD model in this article. This method takes much less time, and each scattering center has a good correspondence with the local structure of the CAD model.

In this article, the P_0 scattering centers obtained above are described with the 3-D attributed scattering center model [8]

$$\begin{aligned} E_i(f, \theta, \phi; \mathbf{z}_i) &= A_i \left(\frac{jf}{f_c} \right)^{\alpha_i} \cdot \sin c \left[2\pi \frac{f L_i}{c} \sin(\phi - \bar{\varphi}_i) \right] \cdot \exp(-k c \gamma_i \sin \phi) \\ &\quad \cdot \exp \left[-j 4\pi \frac{f}{c} (x_i \sin \theta \cos \phi + y_i \sin \theta \sin \phi + z_i \sin \phi) \right]. \end{aligned} \quad (1)$$

In (1), A_i is the amplitude of the i th scattering center, $\mathbf{z}_i = [x_i, y_i, z_i]$ is the 3-D position vector, L_i is the length parameter, and α_i denotes the frequency dependence. ϕ is the aspect angle, and $\bar{\varphi}_i$ is the orientation angle of the distributed scattering center. If the scattering center is localized, $L = 0$, otherwise, $\gamma = 0$. The dependence between ϕ and L of the distributed scattering center can be described by the $\sin c(x)$ function, where $\sin c(x) = \sin(x)/x$. The target's total backscattering field is a sum of the contributions of P_0 individual scattering centers [8], that is,

$$E^s(f, \phi) = \sum_{i=1}^{P_0} E_i^s(f, \theta, \phi; \mathbf{z}_i). \quad (2)$$

Therefore, the scattering center models of the target can be represented by a parameter set $\Theta = \{\Theta_1, \Theta_2, \dots, \Theta_{P_0}\}$, where $\Theta_i = (A_i, \alpha_i, x_i, y_i, z_i, L_i, \gamma_i, \bar{\varphi}_i)$, $i = 1, \dots, P_0$.

B. Automatic and Forward Determination of Physically Relevant Parameters

Once the model form is selected, the problem of establishing parametric models turns into a parameter determination process. The automatic and forward approach to determine physically relevant parameters is another innovation of this article, which focuses on the length parameters and the frequency dependence parameters. The approach is described in detail as follows.

1) Determination of the Length Parameter: The length parameter represents the effective length of the scattering center in the azimuth direction of an SAR image, as well as the dependence of the amplitude on the azimuth angle. The scattering centers can be classified into the localized and the distributed. The localized scattering center shows a bright spot in the SAR image, indicating that the scattering energy is concentrated at this spot, and its length parameter is 0. The flat plate, dihedral, and other typical structures often appear as bright line at specific attitudes in an SAR image. They can form distributed scattering centers, which indicate that the scattering energy is distributed in a certain linear region in the azimuth direction, and the length of the region is the length parameter.

The distributed scattering centers formed by the typical structures reflect the phenomenon of coherent scattering, that is, the amplitude and the phase of the scattering field of these structures satisfy the in-phase coherent condition. However, in complex targets, the strict coherent scattering formed by typical structures is few, and a more common case is approximately coherent scattering formed by surfaces with large

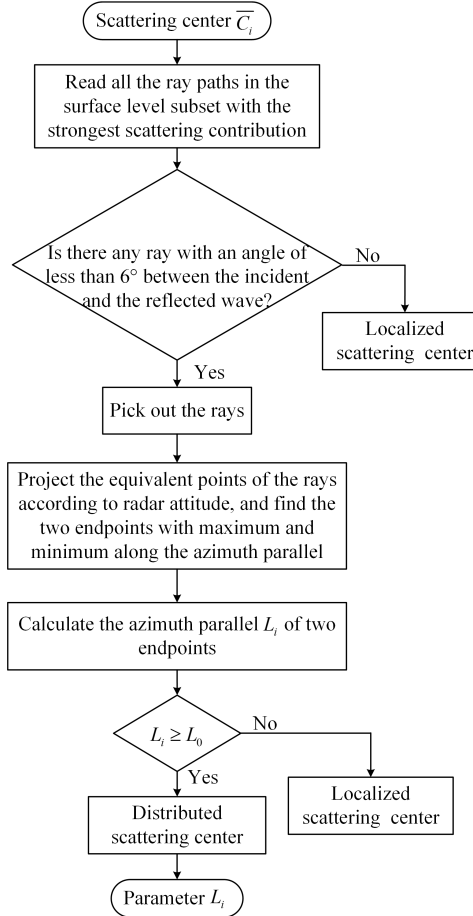


Fig. 3. Flowchart of determining parameter L .

curvature radii, which can also form distributed scattering centers. Therefore, a more general approach is developed to identify and establish distributed scattering center models of curved surfaces with large curvature radii in this article, thus extending the scattering mechanisms of distributed scattering centers from typical scattering structures and specular reflection mechanism to a more general case.

The scattering structures (e.g., the flat plate, dihedral, and ellipsoid with large curvature radii) of distributed scattering centers usually have the characteristics of small surface normal variation. Therefore, from the point of view of scattering characteristics, the scattering field of the distributed scattering center is uniform or nearly uniform in the azimuth direction. Based on the normal provided by the contributive facets, and the given parameters of radar attitude (e.g., azimuth direction), the structures which have such characteristic can be identified; thus, the length parameters are calculated according to the equivalent reflection endpoints of the rays.

The procedure of the automatic and more general approach for determining parameter L is shown in Fig. 3. The steps are as follows. First, during the step of obtaining the component-level and the subcomponent-level ray subsets, the dominant subcomponent-level one is also identified. Then, conditional judgments are done for the rays in the dominant subset. If the field amplitude along each ray is nearly equal and the optical path differences are also nearly equal,

that is to say, the scattering field satisfies nearly coherent scattering, the ray subset may form a distributed scattering center. After projecting the equivalent reflecting points of these rays in the azimuth direction, two equivalent endpoints $Q_m(x_m, y_m, z_m)$, $Q_n(x_n, y_n, z_n)$ can be selected. Finally, a distance L between the two endpoints can be calculated as follows:

$$L = \sqrt{(x_m - x_n)^2 + (y_m - y_n)^2 + (z_m - z_n)^2}. \quad (3)$$

If the value of L projected along the azimuth parallel is greater than or equal to a threshold L_0 , which is equivalent to 2 azimuth resolutions of radar, and the scattering center can be considered as a distributed one, and the length parameter is the distance L ; otherwise, the scattering center is localized. L_0 is as follows:

$$L_0 = \frac{c}{2f \sin\left(\frac{\Delta\phi}{2}\right)} \quad (4)$$

where c is the free-space propagation velocity, ϕ is the aperture angle of the radar, and f is central frequency.

2) Determination of the Frequency Dependence Parameter: The frequency dependence parameter (parameter α) of the scattering center describes the frequency dependence of the amplitude, and this parameter can be determined according to the scattering mechanism of the scattering source. However, the scattering mechanism of complex targets is extremely complicated, and the scattering mechanism of the same component varies with the change in the observation angle. As an example, for a cylinder placed upright, if the incident wave comes from the broadside, the dominant scattering mechanism is the single curve surface reflection, and $\alpha = 0.5$. If the wave comes along the top, the dominant scattering mechanism is the flat reflection, and $\alpha = 1$. For a complex target composed of irregular shapes, it is more difficult to distinguish the scattering mechanism. Therefore, in [24], extensive professional manual analysis for the CAD model is required to distinguish the scattering mechanism at different attitudes, finally determine frequency dependence parameters.

In practice, the frequency dependence parameter can be obtained according to the main scattering mechanism of the scattering center for a complex target, and the main scattering mechanism is closely related to the geometric shape of the dominant subcomponent, which plays a leading role in the scattering of the component. Therefore, the determination of the parameter α turns into the distinction of the surface shape of the dominant subcomponent. In this article, the principal curvature radii are used to distinguish the geometric shape of the dominant region, thus obtaining the main scattering mechanism of the scattering center, and determining the parameter α .

The procedure of automatic and forward approach for determining parameter α is shown in Fig. 4. The detailed steps are as follows.

- 1) Identify the dominant subcomponent-level ray subset of the scattering center during the step to obtain the ray subsets, and obtain the dominant subcomponent according to their path.

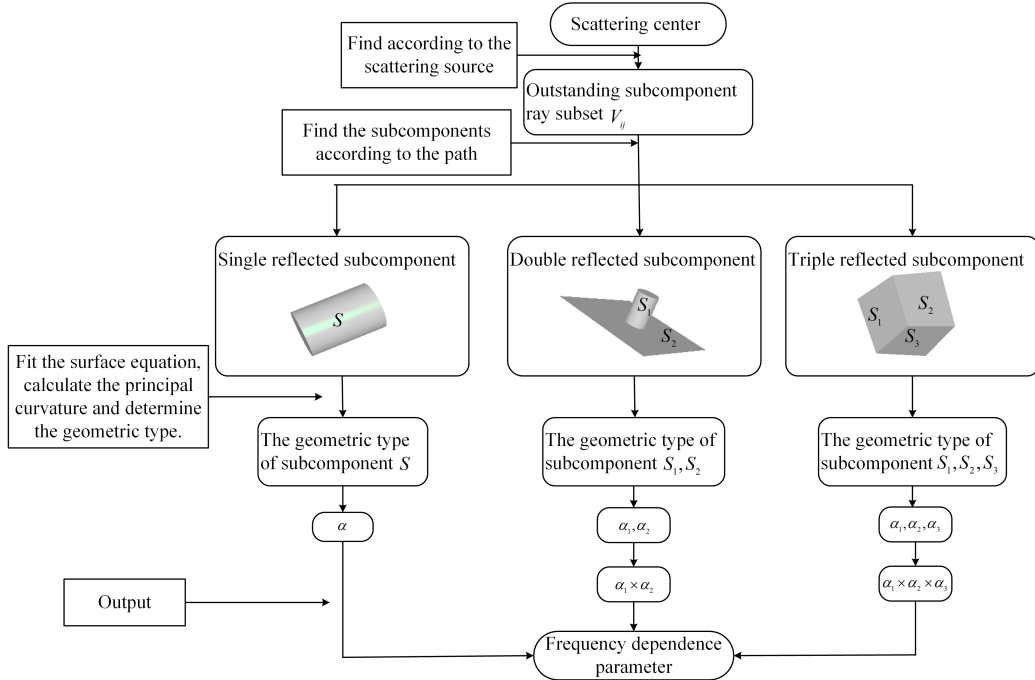


Fig. 4. Flowchart of determining parameter α .

- 2) Calculate the principal curvature radii of the dominant subcomponent.

After obtaining the dominant subcomponent of the scattering center, the principal curvature radii can be calculated by differential geometry theory with the geometric information provided by the facets. The following is known from the conclusion of differential geometry: if the surface equation of subcomponent is expressed as $z = 1/2(Q_{11}x_1^2 + 2Q_{12}x_1x_2 + Q_{22}x_2^2)$, the principal curvature radii $1/\rho$ of an arbitrary point on the surface can be calculated by the following equation:

$$\frac{1}{\rho_{1,2}} = \frac{1}{2} \left[(Q_{11} + Q_{22}) \pm \sqrt{(Q_{11} - Q_{22})^2 + 4Q_{12}^2} \right]. \quad (5)$$

With the 3-D coordinates of the subcomponent facets, the three coefficients Q_{11}, Q_{12}, Q_{22} are fitted by the least square fitting method, thus calculating the principal curvature radii with (5). It should be noted that the patches at the edge are discarded to avoid over-fitting the principal curvature radii.

- 1) Determine the geometric shape of the dominant subcomponent with the principal curvature radii.

In practical applications, due to the limits of electrical dimensions, the mesh of the surface, and the calculation accuracy of the computer, the principal curvature radii calculated in this article often have errors. Generally, the principal curvature radius whose value should be infinite is difficult to reach expect value. After many experiments, it is concluded that if the principal curvature radius is greater than approximately 1000 times of wavelengths, the value can be equal to infinity.

On this basis of the principal curvature radii, the geometric shape of the subcomponent is distinguished as follows.

- 1) If $1/\rho_1$ and $1/\rho_2$ are infinite, the subcomponent is a flat plate.

- 2) If both are finite, the subcomponent is a double curve surface.

- 3) If one is finite and another is infinite, the subcomponent is a single curve surface.

For example, the principal curvature radii of a subcomponent calculated in this article are as follows: $1/\rho_2 = 3.06$ m, $1/\rho_2 = 4780.54$ m. In high-frequency, $1/\rho_2$ is far greater than 1000λ , and it should be equal to infinity. According to the above judgment principle of the surface shape, the subcomponent should be a cylinder.

- 4) Obtain the frequency dependence parameter.

The dominant subcomponent is identified as flat plate, single curve surface or double curve surface (corresponding frequency factor is 1, 0.5, or 0) according to the principal curvature radii, and the frequency dependence parameter can be given as follows: For a single-reflected scattering center, the parameter α is directly determined by the frequency factor, such as a singly curved surface reflection formed by a cylinder, its parameter α is 0.5. For the multiple-reflected scattering center, according to the frequency factor multiplication rule [9], the parameter α is determined by multiplying the frequency factors of all the dominant subcomponents. For instance, a double reflection between flat and singly curved surface formed by a top-hat, and their frequency factors are 0.5 and 1, respectively, thus the parameter α is 0.5. Note that the parameter α of the double reflection between the single curve surfaces does not satisfy the multiplicative relationship.

- 3) *Determination of the Amplitude Parameter and Position Parameter:* The determination approaches of the amplitude and position parameters are introduced in [24], and both approaches are briefly described here.

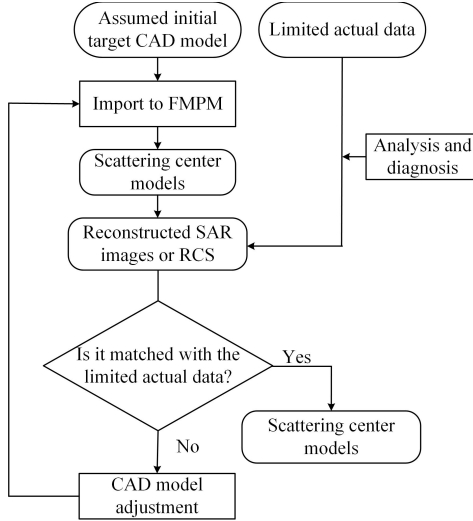


Fig. 5. Flowchart of diagnosing and correcting scattering center models.

The scattering field along each ray can be calculated by hybrid geometrical optics (GO) and PO technique. Here, the contribution of the scattering center is regarded as the sum of the contributions of each ray in the ray subset.

The 3-D position of a scattering center can be determined by weighting the reflection points of all rays in the corresponding subset. For the single-reflected rays, the geometric center of the illuminated facet is regarded as the reflection point. For the multiple-reflected rays, the optical path difference equivalence principle is adopted to obtain the reflection point. And the weight value is determined by the induced current on the target.

Consequently, it is indicated that the method of determining the parameters of the scattering center is a fully forward process, and could provide convenient access to significantly speed up the process to establish the parametric model.

III. DIAGNOSIS AND CORRECTION OF SCATTERING CENTER MODEL

Considering the CAD model of an unknown target is difficult to build, in order to establish its scattering center models, an initial CAD model needs to be assumed based on some limited prior information. Obviously, the scattering center models established from the initial CAD model are difficult to meet the modeling accuracy requirement. However, the modeling method in this article is automatic and rapid, and the correspondence between the scattering center and the scattering structure is much clearer, it will contribute to investigate the scattering characteristic reconstructed by the scattering center models, and correct the scattering center models according to the measured data of the real target. And a technology is studied to diagnose and correct scattering center models of the unknown target.

The procedure of diagnosing and correcting scattering center models is shown in Fig. 5. First, the initial CAD model of target is assumed according to some limited prior knowledge. Then, its scattering center models are generated by the FMPM. The reconstructed SAR images or RCS are compared with the

measurement data. If their similarity meets the requirement, the scattering center models, whose scattering characteristics agree with the measured data, can be output. Otherwise, the initial CAD model needs to be adjusted. The adjustment steps include CAD model scaling, size adjustment of local structure, and increasing-decreasing of local structure. Finally, the scattering center models satisfying accuracy requirements are obtained.

IV. EXAMPLES

In this article, three example targets are presented to demonstrate the validity and efficiency of the automatic and forward modeling method. The first example is the SLICY. The dominant subcomponents and their principal curvature radii are output to show the method can judge the shape of geometric structure, thus demonstrating the method can obtain the frequency dependence parameter correctly. Subsequently, this modeling method extends the formation mechanism of distributed scattering centers from the standard scattering structure and specular reflection mechanism to a more general case, and it does not need complicated manual intervention during obtaining length parameter, so it can effectively establish the parametric models of the modified SLICY, as well as the BMP2. The scattering mechanisms of some scattering centers are analyzed, and it proves that the method correctly determines the model parameters of complex targets. In the fourth example, the technology of scattering center diagnosis and correction is showed through modifying the shapes and configurations of T72 step by step.

Since the MSTAR data set provides only image data for SLICY, T72, and BMP2, to quantitatively illustrate the validity of this method for typical shapes and complex targets, we can evaluate the similarity between the parametric model and the measured data by using two indices, as described in the following.

1) Normalized Similarity of the SAR Images

In fact, the most important feature in SAR target recognition is the structural feature [26]. We use the image similarity, which can characterize the target structures, to measure the accuracy of the parametric model. The similarity is calculated as (6), shown at the bottom of the next page. where $f(x, y)$ is the pixel gray value of the x th row and y th column of the reconstructed SAR image, and $g(x, y)$ is the pixel gray value of the x th row and y th column of the measured image. \bar{f} and \bar{g} denote the mean gray value of the reconstructed and measured SAR images, respectively. Since the two images often differ in space, a translation matching process is required, and Δx and Δy are the shifts in the x - and y - directions. The maximum normalized correlation coefficient Cor is the similarity between the two images.

2) Matching Rate of the Position Parameter

For the parametric scattering center model, the position parameter is also quite important, as this parameter is related to the structural features of the target and describes the phase information of the scattering center.

TABLE I
SCATTERING CENTERS OF SLICY OUTPUT FROM FMPM AT $\theta = 60^\circ$, $\varphi = 0^\circ$, $f = 9.6$ GHz

| Scatterer | A | Outstanding scattering surface | Equivalent canonical geometry | α | L (m) output from FMPM | actual L (m) | 3-D position (m) |
|-------------------|---------|--------------------------------|-------------------------------|----------|-----------------------------|----------------|-------------------|
| $A_4 - A_4$ | 43.4251 | $S_{41} - S_{42}$ | Dihedral | 1 | 1.05 | 1.08 | (0.92,-0.76,0.44) |
| $A_6 - A_6$ | 21.1594 | $S_{61} - S_{62}$ | Dihedral | 1 | 0.49 | 0.52 | (0.92,1.07,0.44) |
| A_5 | 6.9650 | S_{51} | Cylinder | 0.5 | 0.72 | 0.78 | (1.18,0.32,0.59) |
| $A_1 - A_7 - A_7$ | 6.6507 | $S_{31} - S_{71} - S_{72}$ | Trihedral | 1 | 0 | 0 | (0.21,0.38,0.74) |
| $A_2 - A_3$ | 6.6420 | $S_{22} - S_{31}$ | Top-hat | 0.5 | 0 | 0 | (-0.13,0.62,0.75) |
| $A_1 - A_3$ | 5.1546 | $S_{12} - S_{31}$ | Top-hat | 0.5 | 0 | 0 | (0.13,-0.62,0.75) |
| A_3 | 1.2027 | S_{31} | Flat plate | 1 | 0 | 0 | (-0.23,0,0.22) |

We use the position matching rate to further verify the performance of the scattering center model [20]. Here, M is the number of scattering centers, N is the number of peak points extracted by the watershed algorithm from the measured image. M is usually much greater than N . If the Euclidean distance between the scattering center and the peak point is less than 2 pixels, the scattering center is considered to match the peak point. The number of the matched scattering centers is finally counted as M_s , and the matching rate is calculated as follows:

$$p = \frac{M_s}{M}. \quad (7)$$

A. MSTAR SLICY

The first example is the SLICY target. The target's size is $2.45 \text{ m} \times 2.75 \text{ m} \times 1.65 \text{ m}$, its components are cylinder, dihedral, trihedral, quarter cylinder, and other canonical shapes. Considering the CAD model of the SLICY is simple, the index numbers of its components and subcomponents are shown in Fig. 2. The model is disassembled into 7 component parts and 18 subcomponent parts and consists of approximately 21 000 triangular facets.

To obtain the parametric scattering center models, the disassembled CAD model is input into the FMPM. The calculation parameters are set as follows: the zenith angle is 60° , the aspect angle is 0. The plane wave is horizontally polarized with a frequency of 9.6 GHz. And it requires 12 s to obtain the parametric models using a computer with a Core i7 CPU and 4-GB RAM.

The parametric models at $\theta = 60^\circ$, $\varphi = 0^\circ$ are listed in Table I. The FMPM can distinguish the scattering sources and the type of scattering center. The FMPM module judges that three scattering centers are distributed, and the L errors between the output and actual values are small. The scattering mechanisms of all scattering sources are analyzed. The top-hat formed by the double reflection between component A_2 and

component A_3 , and the dominant scattering source is a double reflection between the cylinder's flank and the upper surface of the platform, which are numbered 4 and 5, respectively.

The FMPM module uses the least-squares fitting method to fit the surface equation of the dominant subcomponent. The principal curvature radii of the dominant subcomponent are calculated according to the differential geometry knowledge, and these values are listed in Table II. Four of the radii are infinitely large, so the FMPM judges them to be flat plates. If the principal curvature radius is greater than 1000λ , it should be judged as infinity. When $f = 9.6$ GHz and $1000\lambda = 31.35$ m. The principal curvature radii of the subcomponents numbered 2, 4, and 14 are 209.16, 50.84, and 66.02 m, respectively. According to the judgment principle of the surface shape, the FMPM judges that the three subcomponents are all single curve surfaces.

The SAR image at $\theta = 60^\circ$, $\varphi = 0^\circ$ is reconstructed from the scattering center models and compared with the measurement provided by the MSTAR data set (30_DEG), as shown in Fig. 6. The two images agree well, and the image similarity calculated by (7) is 0.8278. Since the measured environment is rough grass, the measured data contain the scattering contribution from the target, the environment, and the multiple interactions between the target and environment [32]. However, the modeling environment in this article is composed of free space, thus would reduce the image similarity. As shown in Fig. 6 (right), the environmental clutter is very obvious. Fig. 6 (right) shows the source structure corresponding to each scattering center. Due to the multiple interactions between the grassland and the target, the energy distributions of the scattering centers formed by the two dihedrals are dispersive, and the scattering center formed by the long dihedral extracts two peak points by the watershed algorithm. As can be seen from Fig. 7, the positions of the eight peak points extracted from the measured image are taken as the centers of the circles, the radii are equal to 2 pixels (0.5 m), and there are seven scattering centers in the circles.

$$\text{Cor} = \max \left\{ \frac{\sum_x \sum_y [\mathbf{f}(x, y) - \bar{\mathbf{f}}] [\mathbf{g}(x - \Delta x, y - \Delta y) - \bar{\mathbf{g}}]}{\left\{ \sum_x \sum_y [\mathbf{f}(x, y) - \bar{\mathbf{f}}]^2 \sum_x \sum_y [\mathbf{g}(x - \Delta x, y - \Delta y) - \bar{\mathbf{g}}]^2 \right\}^{1/2}} \right\} \quad (6)$$

TABLE II
PRINCIPAL CURVATURE RADII OF OUTSTANDING SURFACES OUTPUT FROM FMPM

| Surface number | Principal curvature radius $\frac{1}{\rho_1}$ (m) | Principal curvature radius $\frac{1}{\rho_2}$ (m) | Shape of surface judged by the FMPM | Is it judged correctly? |
|----------------|---|---|-------------------------------------|-------------------------|
| S_{12} | 0.31 | 209.16 | Single-curved surface | Yes |
| S_{22} | 0.30 | 50.84 | Single-curved surface | Yes |
| S_{31} | ∞ | ∞ | Flat plate | Yes |
| S_{41} | ∞ | ∞ | Flat plate | Yes |
| S_{42} | ∞ | ∞ | Flat plate | Yes |
| S_{51} | 0.31 | 664.02 | Single-curved surface | Yes |
| S_{62} | ∞ | ∞ | Flat plate | Yes |
| S_{61} | ∞ | ∞ | Flat plate | Yes |
| S_{71} | ∞ | ∞ | Flat plate | Yes |

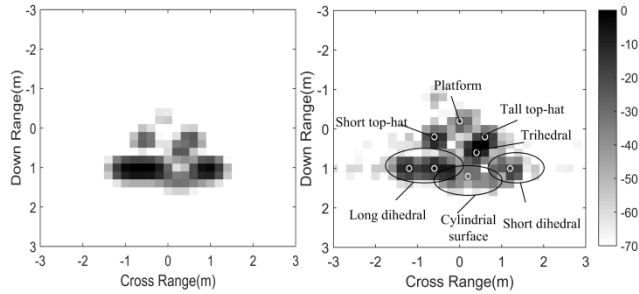


Fig. 6. Comparison between (Left) reconstructed and (Right) actual SAR images for SLICY at $\theta = 60^\circ$, $\varphi = 0^\circ$. The image resolution is $0.25 \text{ m} \times 0.25 \text{ m}$, and the similarity is 0.8278.

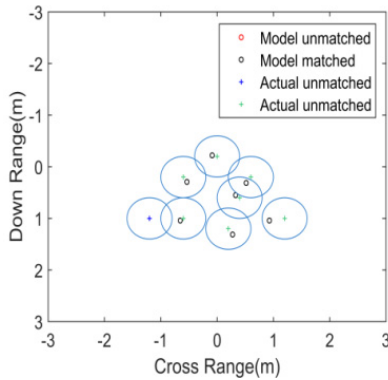


Fig. 7. Matching result of peak points and scattering centers for SLICY at $\theta = 60^\circ$, $\varphi = 0^\circ$, and the position matching rate is 1.

If the peak point extracted from the long dihedral is not considered (the energy distribution is dispersive), the matching rate is 1. The results of image similarity and position matching show that the reconstructed SAR image is in good agreement with the measured image.

B. Modified SLICY

In order to verify that the method expands the formation mechanism of the distributed scattering center, parametric scattering center models of the modified SLICY are established. Fig. 8 shows the CAD model of the modified SLICY, and its

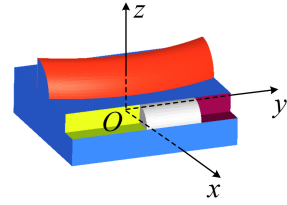


Fig. 8. CAD models of modified SLICY.

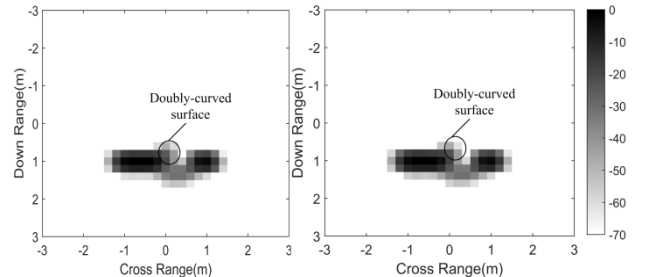


Fig. 9. Comparison between (Left) reconstructed and (Right) simulated SAR image for modified SLICY at $\theta = 60^\circ$, $\varphi = 0^\circ$. The image resolution is $0.25 \text{ m} \times 0.25 \text{ m}$, and the similarity is 0.9990.

components have been differentiated by different colors. The component on the platform is a right-angled fan stretching along an arc with 3 m radius, and other components are the same as the standard SLICY. The modified SLICY is disassembled into 15 components, 16 subcomponents, and approximately 21 000 triangular patches.

We import the modified model into the FMPM, set $\theta = 60^\circ$, $\varphi = 0^\circ$, $f = 9.6$ GHz, and HH polarization, and the parametric models are shown in Table III.

The SAR image is reconstructed from the scattering center models, and a comparison between the reconstructed and reliable simulated SAR images is shown in Fig. 9. It is clearly shown that the amplitudes and positions of the points agree very well, and the similarity between the two images is 0.9990. Since there are many distributed scattering centers, position matching is not adopted here. The simulated SAR image shows that there is a distributed bright spot on the double curve surface position. Because the double curve surface has

TABLE III
SCATTERING CENTERS FOR MODIFIED SLICY OUTPUT FROM FMPM AT $\theta = 60^\circ$, $\varphi = 0^\circ$, $f = 9.6$ GHz

| Scatterer | A | Equivalent canonical geometry | α | L (m) output from FMPM | actual L (m) | 3-D position (m) |
|-----------|---------|--|----------|-----------------------------|----------------|-------------------|
| 3-3 | 42.5273 | Dihedral | 1 | 1.05 | 1.08 | (0.92,-0.76,0.44) |
| 4-4 | 20.4553 | Dihedral | 1 | 0.50 | 0.52 | (0.92,1.07,0.44) |
| 5 | 7.2647 | Cylinder | 0.5 | 0.76 | 0.78 | (1.18,0.32,0.59) |
| 2 | 2.6879 | Doubly-curved surface | 0 | 0.50 | 0.54 | (0.41,0,1.01) |
| 1-2 | 1.7899 | Doubly-curved surface above Flat plate | 0 | 0.50 | 0.54 | (0.50,0,0.22) |

TABLE IV
PARTIAL SCATTERING CENTER RESULTS FOR BMP2 OUTPUT FROM FMPM AT $\theta = 73^\circ$, $\varphi = 93^\circ$, $f = 9.6$ GHz

| Index | Scattering Source | A | Equivalent canonical geometry | α | L (m) | 3-D position (m) |
|-------|-------------------|--------|-------------------------------|----------|---------|--------------------|
| 1 | 23-63 | 1.3378 | Dihedral | 1 | 0 | (0.97,0.07,2.09) |
| 2 | 1-8 | 1.0102 | Dihedral | 1 | 0 | (-0.74,-0.54,1.65) |
| 3 | 15-20 | 1.0097 | Dihedral | 1 | 0 | (0.40,-0.28,2.06) |
| 4 | 1 | 0.9840 | Dihedral | 1 | 0 | (-0.13,1.26,1.47) |
| 5 | 21-21 | 0.9792 | Dihedral | 1 | 0 | (0.39,0.43,2.01) |
| 6 | 28 | 0.9014 | Dihedral | 1 | 0 | (0.04,1.43,1.06) |
| 7 | 2-16 | 0.7239 | Cylinder above flat plate | 0.5 | 0.87 | (-1.72,0.08,1.60) |
| ... | ... | ... | ... | | ... | ... |

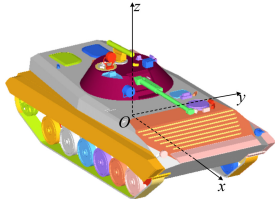


Fig. 10. CAD models of BMP2.

large curvature radii, it forms two distributed scattering centers in the parametric models, and the L parameters are 0.50 m, which is approximately 2 pixels in the SAR image, and the parameter α is 0. The magnitude and position output from FMPM are also equal to those of the simulated SAR. From the above results, the distributed scattering center model formed by curved surfaces with large curvature radii is successfully established by the automatic method of this article.

C. BMP2

Since the modeling method in this article is automatic and rapid, and can establish scattering center models of complex targets with arbitrary shapes, the scattering center models of BMP2 can be established. Fig. 10 shows the CAD model of BMP2, and its components have been differentiated by different colors. The target is sized as 6.72 m \times 3.10 m \times 2.48 m, and it is disassembled into 63 components, 119 subcomponents, and approximately 150 000 triangular facets. The disassembled CAD model is input into the FMPM, and the parameters of the incident wave are set as follows: the zenith angle is 73° , and the aspect angle is 93° . The plane wave is at a frequency of 9.6 GHz and horizontally polarized.

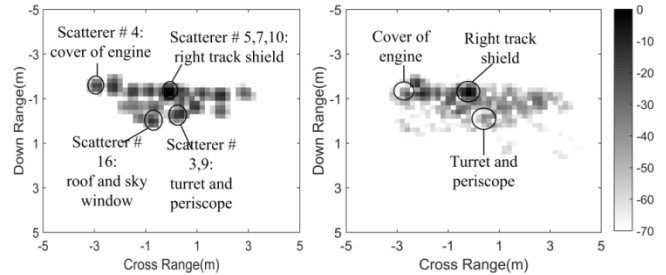


Fig. 11. Comparison between (Left) reconstructed and (Right) actual SAR image for BMP2 at $\theta = 73^\circ$, $\varphi = 93^\circ$. The image resolution is $0.25\text{ m} \times 0.25\text{ m}$, and the similarity is 0.7110.

TABLE V
PARAMETERS FOR RADAR IMAGING

| Polarization | HH | Zenith angle | θ |
|------------------|---------|--------------------|-----------|
| Center Frequency | 9.6 GHz | Aspect angle | φ |
| Bandwidth | 0.6 GHz | Angular Spacing | 0.035° |
| Frequency Step | 5.9 MHz | Synthesis Aperture | 3.5° |
| Range Resolution | 0.25 m | Azimuth Resolution | 0.25m |

On a computer with Core i7 CPU and 4-GB RAM, obtaining the parametric models requires 6 min, and the partial scattering center models are shown in Table IV.

The SAR image is reconstructed from parametric scattering center models, and compared with the actual image from the MSTAR data set (SN_132), as shown in Fig. 11. The imaging parameters are shown in Table V. The similarity between the two images is 0.7110. The 18 peak points are selected from

TABLE VI
PARTIAL SCATTERING CENTER RESULTS FOR T72 OUTPUT FROM FMPM AT $\theta = 73^\circ$, $\varphi = 60^\circ$, $f = 9.6$ GHz

| Index | Scattering Source | A | Equivalent canonical geometry | α | L (m) | 3-D position (m) |
|-------|-------------------|--------|-------------------------------|----------|---------|---------------------|
| 1 | 24-29 | 1.7635 | Cylinder above flat plate | 0.5 | 0 | (0.76, 0.73, 1.16) |
| 2 | 24 | 1.5372 | Single curve surface | 0 | 0 | (0.74, 0.73, 1.43) |
| 3 | 1-24 | 0.6489 | Cylinder above flat plate | 0.5 | 0 | (0.82, 0.71, 1.16) |
| 4 | 40-40 | 0.6316 | Cylinder above flat plate | 0.5 | 0 | (-0.03, 1.04, 0.36) |
| 5 | 38-38 | 0.6101 | Cylinder above flat plate | 0.5 | 0 | (1.21, 1.04, 0.33) |
| 6 | 37-37 | 0.6092 | Cylinder above flat plate | 0.5 | 0 | (1.82, 1.03, 0.38) |
| 7 | 42-42 | 0.6009 | Cylinder above flat plate | 0.5 | 0.87 | (-1.27, 1.04, 0.36) |
| ... | ... | ... | ... | | ... | ... |

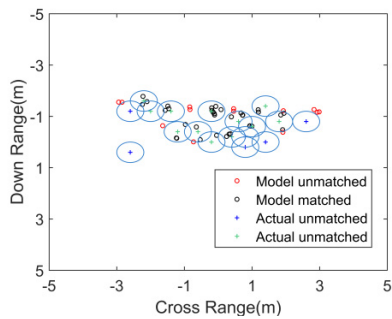


Fig. 12. Matching result of the peak points and the scattering centers for BMP2 at $\theta = 73^\circ$, $\varphi = 93^\circ$, and the position matching rate is 0.7143.

the actual image and matched with the 49 scattering centers output from the FMPM. The 35 scattering centers among them are matched; thus, the matching rate is 0.7143, and the matching result is shown in Fig. 12. The scattering center with the greatest amplitude is derived from the double reflection between the turret and periscope, which forms a dihedral reflector. The peak point with the greatest amplitude in the actual image matches scattering centers #5, 7, and 10, and the peak point is derived from the right wheel cover. Scattering center #4 is derived from the single reflection of the hood, which forms a flat plate reflector, and a peak point in the actual image is matched with this reflector. Scattering center #16 is derived from the double reflection between the roof and the skylight. No peak point in the actual image matched the reflector, which is likely because the geometric model used in this article is different from the actual model.

D. T72

Since the real CAD model of the T72 is difficult to obtain, the established scattering models based on an assumed CAD model are not sufficiently accurate. It is necessary to diagnose and correct the scattering center models by the automatic and forward modeling method.

1) *Initial Model*: Based on the prior knowledge of T72, such as the photograph shown in Fig. 13(a), the initial CAD model is modeled as shown in Fig. 14 (1). Note that it does not meet the accuracy requirement. The model is sized by $7.54 \text{ m} \times 2.52 \text{ m} \times 1.86 \text{ m}$ and consists of approximately 370 000 triangular facets. It is disassembled into 45 components



Fig. 13. (a) Initial model of T72 in this article and (b) possible model of measurement provided by the MSTAR data set.

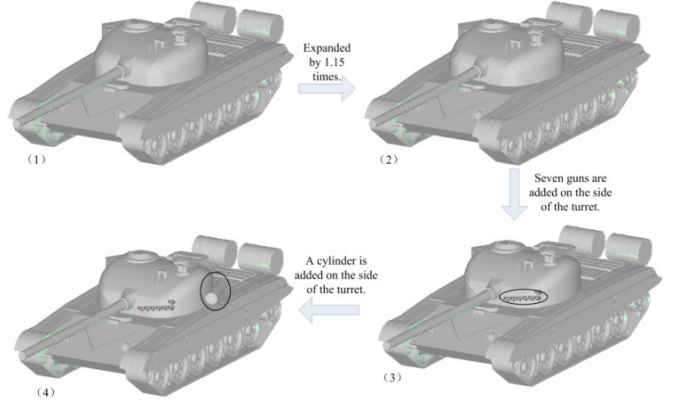


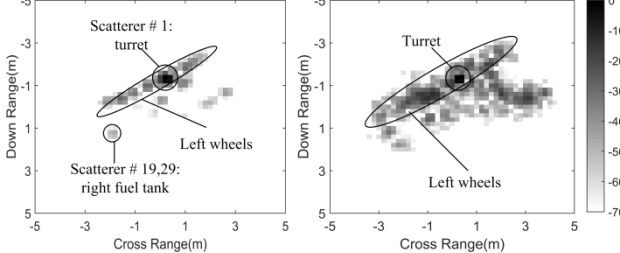
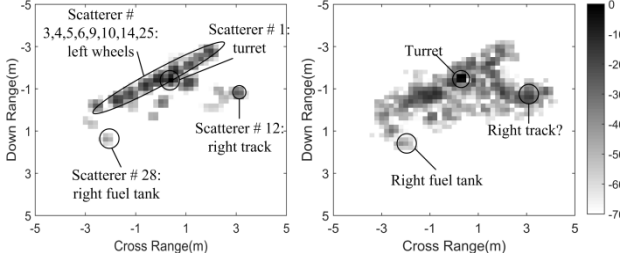
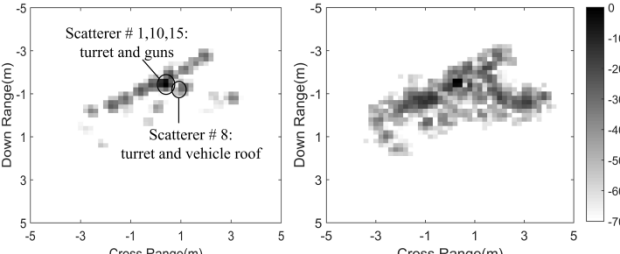
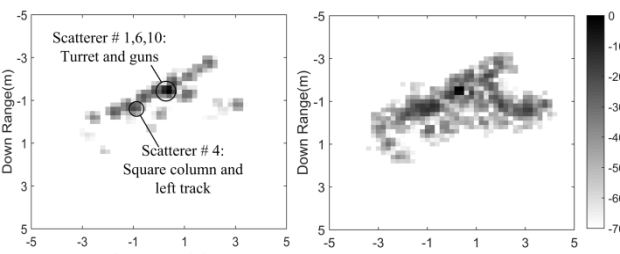
Fig. 14. Geometric modification of T72 model.

and 148 subcomponents, and most of the components are irregular shapes. By comparing and analyzing the image data provided by MSTAR data set, the most possible CAD model is shown in Fig. 13(b). And some modification of the scattering center models is based on the information provided in Fig. 13(b).

We import the initial model into the FMPM, set $\theta = 73^\circ$, $\varphi = 0 \sim 360^\circ$, and $f = 9.6$ GHz, and HH polarization, and the partial scattering center models are shown in Table VI.

We selected the parametric models at $\theta = 73^\circ$, $\varphi = 60^\circ$ and $\theta = 73^\circ$, $\varphi = 159^\circ$, and reconstructed their SAR images. The imaging parameters are shown in Table V. Since the measured environment is rough grass, there are many bright spots with relatively weak brightness in the measured image.

TABLE VII
COMPARISON BETWEEN RECONSTRUCTED AND ACTUAL SAR IMAGES OF T72 MODELS AT $\theta = 73^\circ, \varphi = 60^\circ$

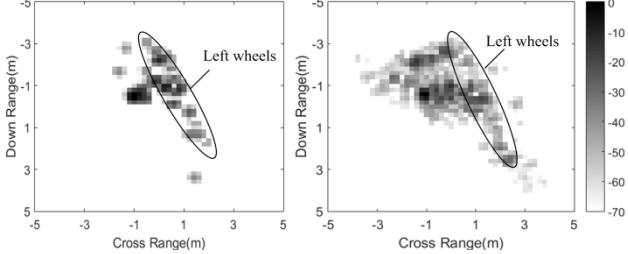
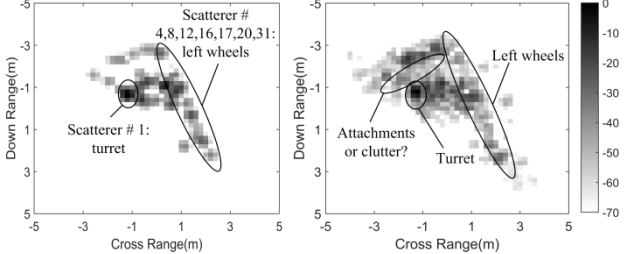
| Model | Reconstructed (left) and actual (right) SAR image | Similarity |
|-----------------|--|------------|
| Initial |  | 0.5449 |
| First Modified |  | 0.7043 |
| Second Modified |  | 0.7240 |
| Third Modified |  | 0.7568 |

The reconstructed SAR image at $\theta = 73^\circ, \varphi = 60^\circ$ is shown in the first row of Table VII, and compared with the actual image from the MSTAR data set (SN_132). The similarity of the two images is 0.5449. The 24 peak points are selected from the actual image and matched with the 38 scattering centers. The 27 scattering centers among them are matched successfully; thus, the matching rate is 0.7105, and the matching result is shown in Table IX. The scattering center with the greatest amplitude is derived from the turret and matched with the peak point marked “turret” in the actual image, and the peak point has the highest brightness. Scattering centers #19 and 29 are derived from the right fuel

drum. Due to the small contribution of the left fuel drum, it is filtered out during parametric modeling. The distribution length of the left wheel in the reconstructed SAR image is significantly shorter than the bright spot marked “left wheels” in the actual image.

The SAR image is reconstructed from the parametric models at $\theta = 73^\circ, \varphi = 159^\circ$ and compared with the actual image from the MSTAR data set (SN_132), as shown in Table VIII. The similarity between the two images is 0.5793. The 24 peak points are selected from the actual image and matched with the 41 scattering centers. The 29 scattering centers are matched successfully, thus the matching rate is 0.7073,

TABLE VIII
COMPARISON BETWEEN RECONSTRUCTED AND ACTUAL SAR IMAGES OF T72 MODELS AT $\theta = 73^\circ, \varphi = 159^\circ$

| Model | Reconstructed (left) and actual (right) SAR image | Similarity |
|----------------|--|------------|
| Initial |  | 0.5793 |
| First Modified |  | 0.7381 |

and the matching result is shown in Table IX. The bright spots on the right side in the reconstructed SAR image are all from the left wheels, and the distribution length is also significantly shorter than the bright spot on the actual image. With the comprehensive analysis of other modeling results, the CAD model used in this article will be expanded by 1.15 times.

2) *First Modification:* As shown in Fig. 14 (2), the initial geometric model is expanded by 1.15 times, and the parametric models are also generated by the FMPM.

We select the parametric scattering center models at $\theta = 73^\circ, \varphi = 60^\circ$, and reconstruct the SAR image. The SAR image is compared with the actual one (which is the same as the right side of the first row and the second column in Table VII), as shown in Table VII. The similarity between the two images is 0.7043. The 24 peak points are selected from the actual image and matched with the 48 scattering centers. The 39 scattering centers are matched successfully. Therefore, the matching rate is 0.8125. The matching result is shown in Table IX. The distribution of the left wheels in reconstructed images is quite similar to the measured image. The scattering center with the greatest amplitude is derived from the turret and matches the peak point marked “turret” in the measured image, but the relative brightness of the scattering center is still lower than that of the measured image. Scattering centers #3, 4, 5, 6, 9, 10, 14, and 25 are derived from the eight left wheels, and the distribution is markedly the same as the measured image. Scattering center #12 is derived from the right wheel cover, and there is also a strong highlight in the measured image. Scattering center #28 is derived from the right fuel drum and has low amplitude, and this scattering center matches the peak point at the “Right fuel drum” in the measured image.

As shown in the second row of Table VIII, the SAR image is reconstructed at $\theta = 73^\circ, \varphi = 159^\circ$ and compared with the actual image (which is in the right side of the first row and the second column in Table VIII). The similarity of the two images is 0.7381. The matching result is shown in Table IX where 18 peak points are extracted from the actual image and matched with the 40 scattering centers. The 34 scattering centers are matched successfully. Therefore, the matching rate is 0.8500. Scattering center #1 with the greatest amplitude is derived from the double reflection between the turret and rear exhaust window. As seen from the second row in Table IX, the peak point with the strongest relative brightness matches scattering center #1. Scattering centers #4, 8, 12, 16, 17, 20, and 31 are derived from the seven left wheels, and the positions of these scattering centers are slightly different from the distribution of the bright points in the actual image. There are many weaker bright spots around the marked “turret” in the actual image. As seen from the photographs provided by the MSTAR data set [e.g., Fig. 13(b)], the geometric models of the turret and the attachments are different from the model used in this article. Therefore, the bright spots should be considered to be derived from the attachments or the multiple interactions between the ground and body parts.

3) *Second Modification:* The similarity between the reconstructed SAR image of the first modified model and the actual image at $\theta = 73^\circ, \varphi = 60^\circ$ is still low. The bright spot marked as “turret” always exists on the actual SAR images at $\theta = 73^\circ, \varphi = 48^\circ - 72^\circ$, and has the greatest brightness. Through an analysis of the parametric models of the first modified model, the bright spot cannot deviate from the double reflection between the turret and vehicle roof. Compared with

TABLE IX
MATCHING RESULTS OF PEAK POINTS AND SCATTERING CENTERS FOR T72 MODELS

| Model | $\theta = 73^\circ, \varphi = 60^\circ$ | | $\theta = 73^\circ, \varphi = 159^\circ$ | |
|----------------|---|------------------------|--|------------------------|
| | Matching result | Position matching rate | Matching result | Position matching rate |
| Original | | 0.7105 | | 0.7073 |
| First Modified | | 0.8125 | | 0.8500 |
| Third Modified | | 0.9120 | | |

the model photographs [e.g., Fig. 13(b)] provided by the MSTAR data set, seven small guns are added on the left side of the turret, as shown in Fig. 14 (3).

The SAR image is reconstructed from parametric models of the second modified model and compared with the actual model (which is the same as the right side of the first row and the second column in Table VII), as shown in Table VII. The image similarity is increased to 0.7240. The scattering mechanism of the gun is the multiple reflection of a cavity. Because only one gun plays a dominant role for the bright spot, the responses of the seven guns can be equivalent to an isotropic bright spot formed by a spherical crown with a flare angle of 18° and a radius of 2.5 m. The amplitude parameter is 3.8630, and the position is (0.4, -1.4).

4) *Third Modification:* After the second modification of the T72 model, the similarity between the reconstructed SAR image and the actual image is significantly increased. However, the geometric model used in this article still has a discrepancy from the actual model, which must be modified for the third time. Compared with the photographs of the possible model provided by the MSTAR data set [e.g., Fig. 13(b)],

a cylinder is added on the left side of the turret, as shown in Fig. 14 (4). The SAR image restructured from the parametric model at $\theta = 73^\circ, \varphi = 60^\circ$ is compared with the actual data. The image similarity is increased to 0.7568, as shown in Table VII. After the third modification, a scattering center is generated, which is formed by the triple reflection among the cylinder, the turret, and the left track. The amplitude parameter is 0.0023, and the position is (-1, -0.6). This scattering center is local, and the bright spot always appears on the actual SAR images at $\theta = 73^\circ, \varphi = 60^\circ \sim 66^\circ$. The 24 peak points are extracted from the actual images at $\theta = 73^\circ, \varphi = 60^\circ$, and matched with 51 scattering centers output from FMPM. The 46 scattering centers are matched, and the matching ratio is 0.9120. The matching result is shown in Table IX.

After the modification of the T72 model, the image similarity and position matching ratio are significantly increased. It can be concluded that, even if the parametric models of a complex target are not precise, these models can be diagnosed and corrected through a step-by-step modification of the CAD model.

V. CONCLUSION

In this article, an automatic and forward method is realized to establish component-level scattering center models directly from the CAD model of the complex target. In addition, the FMPM code is consequently developed based on the method. And the parametric scattering center models of several MSTAR targets are established by the FMPM. In the example of SLICY, the scattering sources and their scattering mechanisms are all listed and analyzed, and the results illustrate the method can correctly output the model parameters of typical shapes. Moreover, the scattering mechanisms of distributed scattering centers are extended from typical structures to curved surfaces by this method and the example of the modified SLICY are given to validate the effectiveness of the extended distributed scattering centers formed by curved surfaces with large curvature radii. Meanwhile, because this method is suitable for complex targets, and avoiding complicated manual intervention, the parametric scattering center models of the BMP2 are established. And compared with the measured SAR images from MSTAR data set, the reconstructed images have high similarity and matching rates.

In addition, a technology is studied to diagnose and correct scattering centers models for a target whose CAD model is unknown or partially known. By gradually modifying the initial CAD model, the automatic and forward method is applied to improve the accuracy of the scattering center models. In the experiment of T72 target, the initial CAD model is scaled and some local structures are changes, and the similarity between the reconstructed SAR images and the measured images is increased from 0.5449 to 0.7568. The experiment represents the potential application of this method for noncooperative targets.

Compared with the previous methods, our modeling method is highly automatic, and the corresponding relationship (geometric structure and scattering mechanism) between the scattering center and its parameters with the CAD model is clear. More research should still be done on parametric modeling for noncooperative targets. Furthermore, the ray tracing technology used in this article considers only the coupling scattering of up to triple reflection. However, for structures with complex scattering mechanisms, such as inlets and cavities, it is necessary to consider the contribution of more than triple bouncing. The automatic and forward method for generating parametric scattering center models may provide an excellent database for SAR ATR, but the research is immature yet, and there is much future work to accomplish.

REFERENCES

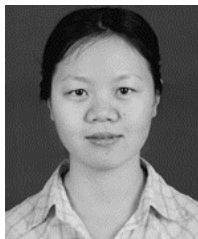
- [1] J. R. Diemunsch and J. Wissinger, "Moving and stationary target acquisition and recognition (MSTAR) model-based automatic target recognition: Search technology for a robust ATR," *Proc. SPIE*, vol. 3370, pp. 481–492, Sep. 1998.
- [2] T. D. Ross, J. J. Bradley, L. J. Hudson, and M. P. O'Connor, "SAR ATR: So what's the problem?—An MSTAR perspective," in *Proc. 6th SPIE-Algorithms Synth. Aperture Radar Imag.*, vol. 3721, Apr. 1999, pp. 662–672.
- [3] R. Hummel, "Model-based ATR using synthetic aperture radar," in *Proc. Rec. IEEE Int. Radar Conf.*, May 2000, pp. 856–861.
- [4] J. Douglas, M. Burke, and G. Ettinger, "High resolution SAR ATR performance analysis," in *Proc. 11th SPIE-Algorithms Synth. Aperture Radar Imag.*, vol. 5427, Sep. 2004, pp. 293–301.
- [5] H.-C. Chiang, R. L. Moses, and L. C. Potter, "Model-based classification of radar images," *IEEE Trans. Inf. Theory*, vol. 46, no. 5, pp. 1842–1854, Aug. 2000.
- [6] M. Martorella *et al.*, "Target recognition by means of polarimetric ISAR images," *IEEE Trans. Aerosp. Electron. Syst.*, vol. 47, no. 1, pp. 225–239, Jan. 2011.
- [7] E. R. Keydel and S. W. Lee, "Signature prediction for model-based automatic target recognition," in *Proc. 3rd SPIE-Algorithms Synth. Aperture Radar Imag.*, vol. 2757, Apr. 1996, pp. 306–317.
- [8] L. C. Potter and R. L. Moses, "Attributed scattering centers for SAR ATR," *IEEE Trans. Image Process.*, vol. 6, no. 1, pp. 79–91, Jan. 1997.
- [9] M. J. Gerry, L. C. Potter, I. J. Gupta, and A. Van Der Merwe, "A parametric model for synthetic aperture radar measurements," *IEEE Trans. Antennas Propag.*, vol. 47, no. 7, pp. 1179–1188, Jul. 1999.
- [10] M. A. Koets and R. L. Moses, "Feature extraction using attributed scattering center models on SAR imagery," *Proc. SPIE*, vol. 3721, pp. 104–115, Aug. 1999.
- [11] M. A. Koets and R. L. Moses, "Image domain feature extraction from synthetic aperture imagery," in *Proc. IEEE Int. Conf. Acoust., Speech, Signal Process. (ICASSP)*, Phoenix, AZ, USA, Mar. 1999, pp. 2319–2322.
- [12] Y. Akyildiz and R. L. Moses, "Scattering center model for SAR imagery," *Proc. SPIE*, vol. 3869, pp. 76–85, Dec. 1999.
- [13] H. Liu, B. Jiu, F. Li, and Y. Wang, "Attributed scattering center extraction algorithm based on sparse representation with dictionary refinement," *IEEE Trans. Antennas Propag.*, vol. 65, no. 5, pp. 2604–2614, May 2017.
- [14] H.-C. Chiang, R. L. Moses, and W. W. Irving, "Performance estimation of model-based automatic target recognition using attributed scattering center features," in *Proc. 10th Int. Conf. Image Anal. Process.*, Sep. 1999, pp. 303–308.
- [15] R. Bhalla and H. Ling, "Three-dimensional scattering center extraction using the shooting and bouncing ray technique," *IEEE Trans. Antennas Propag.*, vol. 44, no. 11, pp. 1445–1453, Nov. 1996.
- [16] R. Bhalla, J. Moore, and H. Ling, "A global scattering center representation of complex targets using the shooting and bouncing ray technique," *IEEE Trans. Antennas Propag.*, vol. 45, no. 12, pp. 1850–1856, Dec. 1997.
- [17] R. Bhalla, H. Ling, J. Moore, D. J. Andersh, S. W. Lee, and J. Hughes, "3D scattering center representation of complex targets using the shooting and bouncing ray technique: A review," *IEEE Antennas Propag. Mag.*, vol. 40, no. 5, pp. 30–39, Oct. 1998.
- [18] Z. Jianxiong, Z. Hongzhong, S. Zhiguang, and F. Qiang, "Global scattering center model extraction of radar targets based on wide-band measurements," *IEEE Trans. Antennas Propag.*, vol. 56, no. 7, pp. 2051–2060, Jul. 2008.
- [19] Z. Jianxiong, S. Zhiguang, C. Xiao, and F. Qiang, "Automatic target recognition of SAR images based on global scattering center model," *IEEE Trans. Geosci. Remote Sens.*, vol. 49, no. 10, pp. 3713–3729, Oct. 2011.
- [20] J. A. Jackson, B. D. Rigling, and R. L. Moses, "Canonical scattering feature models for 3D and bistatic SAR," *IEEE Trans. Aerosp. Electron. Syst.*, vol. 46, no. 2, pp. 525–541, Apr. 2010.
- [21] D. F. Fuller and M. A. Saville, "A high-frequency multipole model for wide-angle SAR imagery," *IEEE Trans. Geosci. Remote Sens.*, vol. 51, no. 7, pp. 4279–4291, Jul. 2013.
- [22] J. Zhu, S. Tan, J. King, C. Derksen, J. Lemmettyinen, and L. Tsang, "Forward and inverse radar modeling of terrestrial snow using SnowSAR data," *IEEE Trans. Geosci. Remote Sens.*, vol. 56, no. 12, pp. 7122–7132, Dec. 2018.
- [23] J. B. Keller, "Geometrical theory of diffraction," *J. Opt. Soc. Amer.*, vol. 52, no. 2, pp. 116–130, Feb. 1962.
- [24] Y. He, S.-Y. He, Y.-H. Zhang, G.-J. Wen, D.-F. Yu, and G.-Q. Zhu, "A forward approach to establish parametric scattering center models for known complex radar targets applied to SAR ATR," *IEEE Trans. Antennas Propag.*, vol. 62, no. 12, pp. 6192–6205, Dec. 2014.
- [25] B. Ding and G. Wen, "A region matching approach based on 3-D scattering center model with application to SAR target recognition," *IEEE Sensors J.*, vol. 18, no. 11, pp. 4623–4632, Jun. 2018.
- [26] B. Ding and G. Wen, "Target reconstruction based on 3-D scattering center model for robust SAR ATR," *IEEE Trans. Geosci. Remote Sens.*, vol. 56, no. 7, pp. 3772–3785, Jul. 2018.
- [27] X. L. Yang, G. J. Wen, J. R. Zhong, B. W. Hui, and C. H. Ma, "A 3-D electromagnetic-model-based algorithm for absolute attitude measurement using wideband radar," *IEEE Geosci. Remote Sens. Lett.*, vol. 12, no. 9, pp. 1878–1882, Sep. 2017.

- [28] X. Yang, G. Wen, C. Ma, S. Qiu, and B. Ding, "Three-dimensional electromagnetic model-based pose estimation using fully polarimetric wideband radar," *IEEE Geosci. Remote Sens. Lett.*, vol. 13, no. 8, pp. 1054–1058, Aug. 2016.
- [29] X. Yang, G. Wen, C. Ma, and B. Hui, "Three-dimensional electromagnetic-model-based absolute attitude measurement using monostatic wideband radar," *J. Appl. Remote Sens.*, vol. 11, no. 1, Feb. 2017, Art. no. 015015.
- [30] F. Weinmann, "Ray tracing with PO/PTD for RCS modeling of large complex objects," *IEEE Trans. Antennas Propag.*, vol. 54, no. 6, pp. 1797–1806, Jun. 2006.
- [31] R. Touzi, "A review of speckle filtering in the context of estimation theory," *IEEE Trans. Geosci. Remote Sens.*, vol. 40, no. 11, pp. 2392–2404, Nov. 2002.
- [32] S. Chen, H. Wang, F. Xu, and Y.-Q. Jin, "Target classification using the deep convolutional networks for SAR images," *IEEE Trans. Geosci. Remote Sens.*, vol. 54, no. 8, pp. 4806–4817, Aug. 2016.



Jin Liu was born in Huanggang, Hubei, China, in 1990. He received the B.S. degree in electronic and information engineering from Wuhan Textile University, Wuhan, China, in 2014. He is pursuing the Ph.D. degree with the School of Electronic Information, Wuhan University, Wuhan.

His research interests include electromagnetic scattering, complex objects characterizing, and radar imaging.



Siyuan He (Member, IEEE) was born in Jinhua, Zhejiang, China, in 1982. She received the B.S. degree in telecommunication engineering and the Ph.D. degree in radio physics from Wuhan University, Wuhan, China, in 2003 and 2009, respectively.

From 2005 to 2006, she was a Research Assistant with the Wireless Communications Research Center, City University of Hong Kong, Hong Kong. From 2009 to 2011, she was a Post-Doctoral Researcher with Wuhan University. She is currently a Full Professor with the School of Electronic Information, Wuhan University. Her research interest includes electromagnetic theory and its application, computational electromagnetism, radar imaging, and electromagnetic inverse scattering.



Lei Zhang was born in Lianyungang, Jiangsu, China, in 1991. He received the B.S. degree in electronic and information engineering from Shandong University, Jinan, China, in 2014. He is pursuing the Ph.D. degree with the School of Electronic Information, Wuhan University, Wuhan, China.

His research interests include electromagnetic scattering, complex objects characterizing, radar imaging, and synthetic aperture radar automatic target recognition.



Yunhua Zhang was born in Ezhou, Hubei, China, in 1981. He received the B.S. and M.S. degrees in electronic engineering from Wuhan University, Wuhan, China, in 2003 and 2006, respectively, and the Ph.D. degree in electronic engineering from the University of Leeds, Leeds, U.K., in 2011.

From 2010 to 2012, he was a Post-Doctoral Researcher with the Queen's University of Belfast, Belfast, U.K. After that, he was an Associate Professor with Wuhan University. His research interest includes antennas, metamaterials and their applications, and computational electromagnetism.



Guoqiang Zhu (Member, IEEE) was born in Wuhan, China, in 1959. He received the B.S., M.S., and Ph.D. degrees in radio physics from Wuhan University, Wuhan, in 1982, 1985, and 1997, respectively.

He is a Professor with the School of Electronic Information, Wuhan University. He has authored over 60 journal articles. His research interest includes complex objects characterizing, electromagnetic scattering and radiation, electromagnetic theory, and numerical techniques.



Hongcheng Yin was born in 1967. He received the B.S. degree in electromagnetic field and microwave technique from Northwest Telecommunication Engineering Institute, Xi'an, China, in 1986, the M.S. degree in electromagnetic field and microwave technique from the Beijing Institute of Environmental Features (BIEF), Beijing, China, in 1989, and the Ph.D. degree in electromagnetic field and microwave technique from Southeast University, Nanjing, China, in 1993.

From 1989 to 1990, he was an Assistant Engineer with the Microwave Laboratory, BIEF. From 1993 to 1995, he was a Post-Doctoral Research Fellow with the University of Electronic Science and Technology of China, Chengdu, China. From 1995 to 2001, he was a Senior Engineer with the PLA Air Force Radar Research Institute, Beijing. Since 2001, he has been a Researcher with the Science and Technology on Electromagnetic Scattering Laboratory, China Aerospace Science and Industry Corporation, Beijing. His research interests include numerical methods in electromagnetic fields, electromagnetic scattering, inverse scattering, and propagation.

Dr. Yin is a fellow of the Chinese Institute of Electronics.



Hua Yan was born in Harbin, Heilongjiang, China, in 1981. He received the B.S. and M.S. degrees in physics from the Beijing Institute of Technology, Beijing, China, in 2004 and 2007, respectively. He is pursuing the Ph.D. degree in electromagnetic field and microwave technology with the Communication University of China, Beijing.

From 2007 to 2011, he was an Assistant Engineer with the Science and Technology on Optical Radiation Laboratory, Beijing. Since 2011, he has been a Senior Engineer with the Science and Technology on Electromagnetic Scattering Laboratory, Beijing. His research interest includes the electromagnetic scattering modeling and parametric modeling.